agriculture

MDPI

Article

A Specific Time Lag Regulation of Soil Moisture Across Layers on Soil Salinization in the Northeast Tibetan Plateau Agroecosystem

Di Wei [1,†], Ziqi Zhang [1,†], Lin Yan [1], Jia Yu [1], Yun Zhang [1,2,*] and Bo Wang [1]

[1] Key Laboratory of Western China's Environmental Systems (Ministry of Education), College of Earth and Environmental Sciences, Lanzhou University, Lanzhou 730000, China; weid20@lzu.edu.cn (D.W.); zhziqi2023@lzu.edu.cn (Z.Z.); 220220948470@lzu.edu.cn (L.Y.); yuj2023@lzu.edu.cn (J.Y.); wangbo@lzu.edu.cn (B.W.)

[2] Ministry of Education Engineering Research Center of Water Resource Comprehensive Utilization in Cold and Arid Regions, Lanzhou 730000, China

* Correspondence: zhangyun@lzu.edu.cn

† These authors contributed equally to this work.

Abstract: The evaporation of soil water drives the upward movement of salt and its accumulation on the surface, which ultimately leads to soil salinization in agroecosystems. With the rapid development of remote sensing technology, the soil water and salt transport can be monitored accurately. Based on Landsat 8 satellite imagery and ERA5-Land reanalysis datasets, this study explored the variation characteristics of soil water and salt in the northeast Tibetan Plateau from 2013 to 2023, inferred by geostatistical methods like ridge regression, windowed cross correlation, and machine learning algorithms. The results show that the negative correlation effect between deep soil moisture (100–289 cm) and soil salinization is stronger. Moreover, soil water and salt also have a time lag effect compared with instant responses, meaning that the soil salinization caused by deep soil moisture may require longer transport times. As the potential driving factors, an increase in soil organic carbon and runoff is beneficial for alleviating salinization while abundant runoff also promotes soil humidification. This study has elucidated the specific regulation of soil salinization by soil moisture within different profiles, which is beneficial for understanding the ecological balance of soil water and soil salt in agroecosystems.

Keywords: soil salinization; soil moisture; agroecosystem dynamic change; remote sensing image; Tibetan Plateau

Received: 5 December 2024
Revised: 3 January 2025
Accepted: 3 January 2025
Published: 5 January 2025

Citation: Wei, D.; Zhang, Z.; Yan, L.; Yu, J.; Zhang, Y.; Wang, B. A Specific Time Lag Regulation of Soil Moisture Across Layers on Soil Salinization in the Northeast Tibetan Plateau Agroecosystem. *Agriculture* **2025**, *15*, 106. https://doi.org/10.3390/agriculture15010106

1. Introduction

Soil salinization caused by the imbalance of water and salt transport processes is one of the key limiting constraints of agroecosystems [1], which refers to the gradual accumulation of soluble salts on the soil surface [2]. Global warming accelerates the upward movement of water-soluble ions in soil, leading to an inevitable salinization and dramatically dwindled agricultural water resource [3]. It has adverse effects on nutrient availability and plant growth, leading to crop reduction and land desertification [4]. Meanwhile, agricultural soil salinization leads to a negative socio-economic impact on environmental health and human well-being [5]. The accompanying degradation of forage in the plateau ecosystem will increase the cost of ecological restoration and cause an imbalance in the alpine plateau agroecosystem [6]. These both call for an attention to the soil salinization of agroecosystems due to its ecological importance.

Soil salinization is a significant global issue, particularly severe in Asia, where large areas of land are affected [7]. It is mainly caused by factors such as climate, topography, and

soil properties. For example, in arid and semi-arid regions with high temperatures, intense evaporation, and low precipitation, salts tend to accumulate in the soil [8]. Soil moisture, on the other hand, is crucial in the hydrological cycle and affects many processes at the land–atmosphere interface [9]. There is a complex interaction between soil salinization and soil moisture. High soil moisture may lead to the leaching of salts in certain areas, reducing soil salinity. However, in other situations, excessive soil moisture can also cause problems like waterlogging, which may in turn affect the solubility and migration of salts [10]. Conversely, soil salinization can also impact soil moisture characteristics. The presence of salts can change the physical and chemical properties of the soil, altering its water-holding capacity and infiltration rate [11]. All in all, understanding the relationship between soil salinization and soil moisture is essential for effective land management and sustainable agricultural development.

In recent decades, the advancement of remote sensing technologies has revolutionized how we monitor the environment and changes in global ecosystems [12]. This progress, coupled with the development of machine learning technology, helps us better explore the dynamic changes in the pedosphere [13], which has made it possible to capture the spatiotemporal variation characteristics of soil water and salt transport on a large scale [14]. Scholars and practitioners obtain high-resolution data by interpreting satellite imagery [15], informing sustainable agricultural management decisions and strategies [16]. Normally, the surface reflection radiation band in satellite imagery is used to extract soil characteristics [17] and then the moisture content, organic matter, and salt content are calculated through a prediction model [18]. Moreover, integrating remote sensing data with other data (such as reanalysis datasets) can achieve more accurate soil ecological information by complementing each other's strengths and limitations [19]. It can be obviously seen that the significant growth of remote sensing technology has solved many problems for the ecological assessment of soil water and salt elements, including high data resolution, wide spatiotemporal coverage, convenient processing costs, etc. [20].

Most published studies have demonstrated the feasibility of using remote sensing techniques to explore soil salinization and its ecological regulation. The use of quantitative indicators from different datasets to construct feature space inversion models with multiple dimensions is gradually becoming the mainstream tool for soil salinization assessment [21]. Seifi et al. [19] used Landsat image spectral data as input variables and combined partial least squares regression to predict soil salinity, which showed a high degree of agreement with field sampling results. Ding et al. [22] extracted soil moisture data from remote sensing images of an arid oasis and found a good correlation with surface soil salinity. Bian et al. [23] constructed a feature space model based on surface albedo to quantify the relationship between soil salinity and surface parameters, which has strong predictive power. Jiang et al. [24] developed a soil salinity inversion model using multi-source remote sensing data, demonstrating that the vegetation moisture coefficient is an important regulating variable for soil salinity.

The ecological impact of soil salinization is often characterized in the coupling space between vegetation greenness and soil salt. To quantitatively describe the coupling space, the spectral index has been used among many researchers, which is a combination of pixel values from specific spectral bands [25]. Compared with the variance in reflectance between the near-infrared red band (NIR), red band (R), and blue band (B), it is proven to be useful in soil salinization detection [26]. The studies conducted in the Qom Valley and the Great Hungarian Plain both have demonstrated the excellent performance of multi-spectral data in predicting soil salinization, with an accuracy rate of over 75% [27]. It can be concluded that in recent years, the research focus on soil salinization detection has shifted from traditional field investigation to remote sensing spectral data analysis.

The northeastern part of the Tibetan Plateau has three typical inland river basins, which are ecologically fragile and climate-sensitive, resulting in complex changes in soil water and salt elements, and they are often prone to soil degradation processes such as soil salinization [28]. Therefore, the regulation of soil moisture across layers on the soil salinization of the northeast Tibetan Plateau has been explored in this study to better describe the regional characteristics of soil water and salt transport. After clarifying the variation pattern through trend test, ridge regression and windowed cross correlation were applied to determine the time lag effect of dominant soil moisture and, ultimately, potential driving factors were identified by a machine learning algorithm. This study is beneficial for understanding the characteristics of soil water and salt cycling at the regional scale, providing a scientific basis and theoretical reference for sustainable agricultural development.

2. Method and Materials

2.1. Study Area

The rock soil parent material in the Tibetan Plateau contains a significant amount of salt, which is gradually released into the soil through long-term geological processes such as weathering and leaching [29]. In addition, the scarce precipitation in the Tibetan Plateau and the strong evaporation caused by drought jointly result in the continuous accumulation of salt in groundwater on the surface, ultimately leading to soil salinization [30]. As an important river source area in northwest China, the regulation of water and salt transport processes in the northeast Tibetan Plateau is relatively complex due to the influence of underlying surface conditions in cold regions such as glaciers, permafrost, and snow cover [31]. Three typical river basins located in the northeast Tibetan Plateau are selected as the study area (Qaidam, Hexi, Yellow), with an altitude from 1763 m to 6474 m, as shown in Figure 1. The climate type belongs to the plateau temperate zone, with the highest monthly average temperature being above 10 degrees Celsius, the water supply decreasing from southeast to northwest, and the even seasonal distribution of light resources [32]. The unique climatic conditions render it an area with a high concentration of agriculture, forestry, and animal husbandry on the Tibetan Plateau [33].

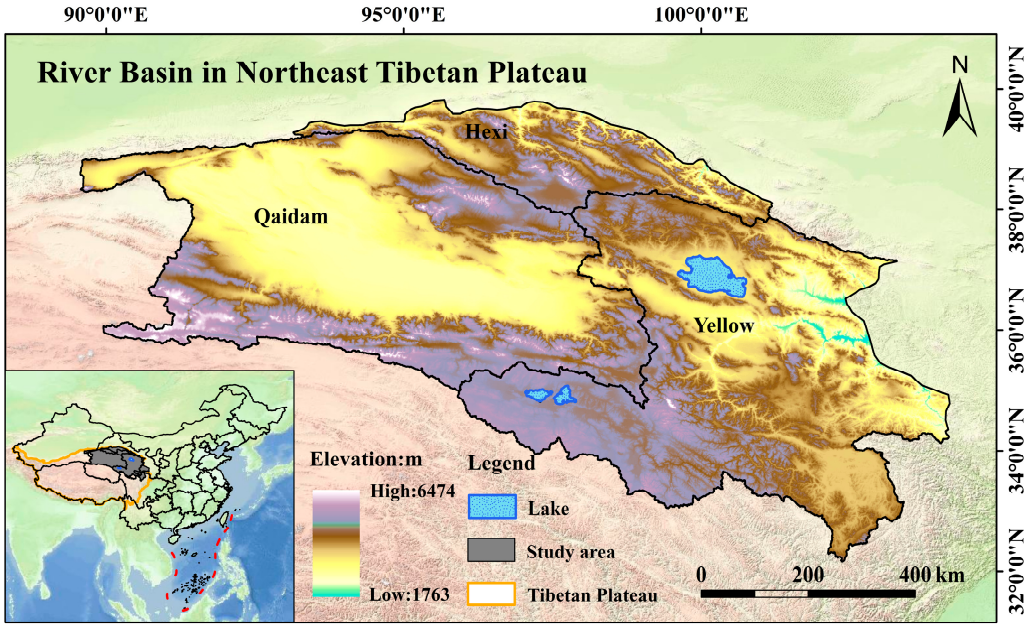

Figure 1. The geographical location of the study area.

2.2. Data Sources and Preprocessing

As for soil salinization and soil moisture, the Landsat 8 OLI scenes and the ERA5-Land reanalysis dataset can provide the most forward-looking data, ensuring research for the latest period from 2013 to 2023 can be conducted. A series of consecutive Landsat 8 OLI scenes covering this specific area and period were selected, which were rectified to the Universal Transverse Mercator (UTM) coordinate system using the World Geodetic System (WGS) 1984 datum allocated to the UTM Zone 44N [34]. After preprocessing, several reflectances of single bands were extracted, including the near-infrared band, the red band, and the blue band. Meanwhile, with the help of the Copernicus Climate Change Service, the ERA5-Land reanalysis dataset was used to acquire the soil moisture across layers with homology [35], providing the soil moisture across layers at a spatial resolution of 0.1° as follows [36]: Level 1 (0–7 cm), Level 2 (7–28 cm), Level 3 (28–100 cm), and Level 4 (100–289 cm).

Additionally, the boundary data of the Tibetan Plateau came from the National Tibetan Plateau/Third Pole Environment Data Center (http://data.tpdc.ac.cn, accessed on 20 April 2024), while the river basin dataset was provided by the National Cryosphere Desert Data Center (http://www.ncdc.ac.cn, accessed on 20 April 2024). When considering potential driving factors, climate elements were also obtained from the ERA5-Land monthly averaged data from 1950 to present (https://cds.climate.copernicus.eu, accessed on 30 May 2024) and soil texture data were taken from the Harmonized World Soil Database version 2.0 (https://gaez.fao.org/pages/hwsd, accessed on 30 May 2024).

In order to quantitatively characterize soil salinization based on multi-band remote sensing images, it was necessary to define a salinization detection index (SDI) inferred by the feature relationship between the normalized difference vegetation index (NDVI) and salinity index (SI) [26], calculated by Formulas (1) and (2) [37].

$$NDVI = \frac{\rho_{nir} - \rho_{red}}{\rho_{nir} + \rho_{red}} \quad (1)$$

$$SI = \sqrt{\rho_{red} \times \rho_{blue}} \quad (2)$$

where ρ_{nir}, ρ_{red}, and ρ_{blue} are the reflectances of the corresponding band of Landsat images, respectively. Based on the Google Earth Engine (GEE) platform, Landsat 8 OLI images within the spatiotemporal range of this study have been screened, and quality control conditions (including radiometric correction, atmospheric correction, and cloud correction) were added to extract surface reflectance data for different bands. Due to that, the NDVI is the normalized difference between the near-infrared band and red band; the *normalizedDifference* function of GEE is used to calculate the NDVI and generate new raster images. Similarly, the arithmetic square root of the product of red band reflectance and blue band reflectance is used to calculate the salinity index.

In the two-dimensional feature space trajectory of vegetation greenness and soil salt, there is a significant nonlinear relationship between the NDVI and SI, and the distance to the extremum point can indicate the degree of soil salinization, where the extremum point means that the NDVI achieves 1 and the SI achieves 0. The NDVI and SI obtained from spectral data are used to calculate the SDI, as shown in Formula (3) [26].

$$SDI = \sqrt{(NDVI - 1)^2 + SI^2} \quad (3)$$

The spectral reflectance from original Landsat 8 OLI images with a spatiotemporal resolution of 16 days and 30 m is synthesized to a monthly scale and resampled to a spatial resolution of 1 km. At the same time, a bilinear interpolation towards 1 km has also been

performed on soil moisture data from the ERA5-Land meteorological reanalysis dataset to ensure consistent resolution.

2.3. Geostatistical Methods

2.3.1. Spatiotemporal Variation

The spatial characteristics of soil water and salt elements during the study period were determined using Sen's slope trend test [38], expressed as Formula (4).

$$\theta = mean\left(\frac{x_j - x_i}{j - i}\right), j > i \tag{4}$$

where θ is the calculated Sen's slope and x_i and x_j are the values at times i and j within the dataset. In addition, a two-tailed t-test is used to verify the robustness, and the results with $p < 0.05$ are defined as significant variation trends at a 95% confidence interval.

Meanwhile, the Z-score standardization method was used to observe the temporal changes in time-series data, expressed as Formula (5).

$$\epsilon_{standardized} = \frac{\epsilon - \mu}{\sigma} \tag{5}$$

where ε refers to time-series data, μ is the average value, and σ is the standard deviation. The calculated $\varepsilon_{standrdized}$ can standardize the raw data, that is, convert it into a dimensionless relative position to the mean so that comparisons can be made among different datasets.

2.3.2. Quantitative Contribution

Multiple linear regression can quantify the impact of soil moisture across layers on surface salinization [39], expressed as Formulas (6) and (7).

$$SDI = \sum_{m=1}^{n} \beta_m x_m + b \tag{6}$$

$$\beta = \left(X^T X\right)^{-1} X^T y \tag{7}$$

where each x_m represents a normalized independent variable aiming for the normalized SDI, which refers to soil moisture across layers in this study; n denotes the total number of variables; b is the constant term; X is a correlation matrix while y is a scalar of the matrix; and β is the regression coefficient of the linear regression model.

Ridge regression was used to determine the relative and absolute contribution rates of each soil moisture to the SDI [40]; moreover, the dominant factors were identified by comparing the contribution rates [41] and can be calculated together.

$$Y_m = \sum_{i=1}^{n} a_i X_{im} + d \tag{8}$$

$$\eta_{c1} = a_1 \times X_{1s\_trend} \tag{9}$$

$$\eta_{rc1} = \frac{|\eta_{c1}|}{|\eta_{c1}| + |\eta_{c2}| + |\eta_{c3}| + \cdots} \tag{10}$$

$$\eta_{ac} = \frac{\eta_{c1}}{Y_{n\_trend}} \times Y_{trend} \tag{11}$$

where Y_m is the normalized dependent variable, X_{im} is the normalized independent variables, a_i is the regression coefficient, d is the residual, X_{1s_trend} is the variation trend in the first variable, and Y_{trend} and Y_{n_trend} are the variation trends in specific dependent variables

and all dependent variables, respectively. Finally, η_{rc1} is the relative contribution and η_{ac} is the absolute contribution amount.

2.3.3. Windowed Cross Correlation

The windowed cross correlation (WCC) method was developed to analyze the association between cyclically varying covariates with a time effect [42]. When generic variable B responds within a certain period of time after generic variable A changes, it can be considered that B lags behind A and vice versa [43]. Therefore, the cross correlation of two time-series datasets (X, Y) is given by

$$r(X, Y, m) = \frac{1}{N-m} \sum_{i=1}^{N-m} \frac{\left(X_i - \overline{X}\right)\left(Y_i - \overline{Y}\right)}{var(X)\ var(Y)} \tag{12}$$

where m denotes the lag window in months within N. X and Y represent two variables, while $var(X)$ and $var(Y)$ mean the standard deviations, respectively.

2.3.4. Statistical Machine Learning

As a robust tool for driving factor identification in geostatistical methods, the random forest algorithm of machine learning evaluates the importance of each feature by reducing the impurity caused during the construction of decision trees, which divided the dataset by bootstrap resampling and calculated the mean decrease accuracy (MDA) across all decision trees [44,45].

Additionally, the SHapley Additive exPlanation (SHAP) is utilized to evaluate the concise causality relationships between feature variables and is often used for further descriptions of black box models such as random forests [46]. The SHAP method has been widely adopted due to its ideal characteristics, including local accuracy, omission, and consistency [47]. The bee colony graph obtained by SHAP analysis can display the global distribution of feature variables and sort the feature variables from high to low according to the average SHAP value.

3. Results

3.1. Interannual Trend

The interannual variation in the calculated SDI of the river basin in the northeast Tibetan Plateau is investigated, as shown in Figure 2. In Figure 2a, it can be seen that the extent of soil salinization roughly increases from southeast to northwest; more than 80% of the areas in the Qaidam River Basin exhibit severe salinization or above, while nearly 75% of the areas in the Yellow River Basin are still at a relatively low risk of salinization. Unlike the significant spatial pattern presented by these two basins, Hexi River Basin remains consistent with the overall study area, manifested as a multi-level distribution of soil salinization. Figure 2b shows the trend in soil salinization during the study period. The extent of soil salinization in the northeast Tibetan Plateau has slightly increased from 2013 to 2023, with an average rate of 0.0079 decade^{-1}. Meanwhile, from the perspective of basin differentiation, areas with severe soil salinization are gradually weakening, while areas with mild levels are worsening. Interestingly, the most notable increase is located at the junction of the Hexi River Basin and the Yellow River Basin.

The interannual average and variation trend in soil moisture across layers are shown in Figures 3 and 4. Accompanied by an increase in depth, soil moisture fluctuates and increases from 0.2566 m^3/m^3 to 0.2874 m^3/m^3, meaning the deep soil becomes more humid. The multi-year average of soil moisture values between basins are Qaidam, Hexi, and Yellow in ascending order, which is exactly opposite to the soil salinization extent. Except for the Yellow River Basin, where all soil layers show an increasing trend in soil

moisture, other basins and the whole study area have experienced a gradation of first drying and then wetting along the soil profile. The soil layer with abrupt changes between basins is different, and the whole study area undergoes changes in the Level 2 layer, while in Qaidam River Basin, it is the Level 3 layer; eventually, Hexi River Basin shows a Level 4 layer below the crop root zone.

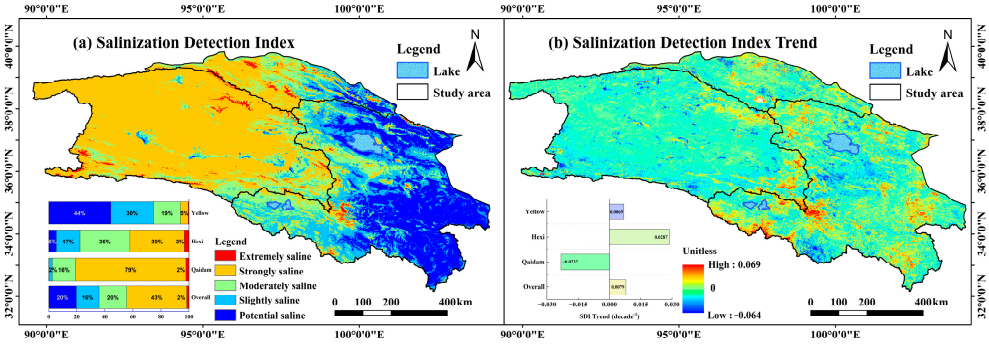

Figure 2. Multi-year average and variation trend in salinization detection index.

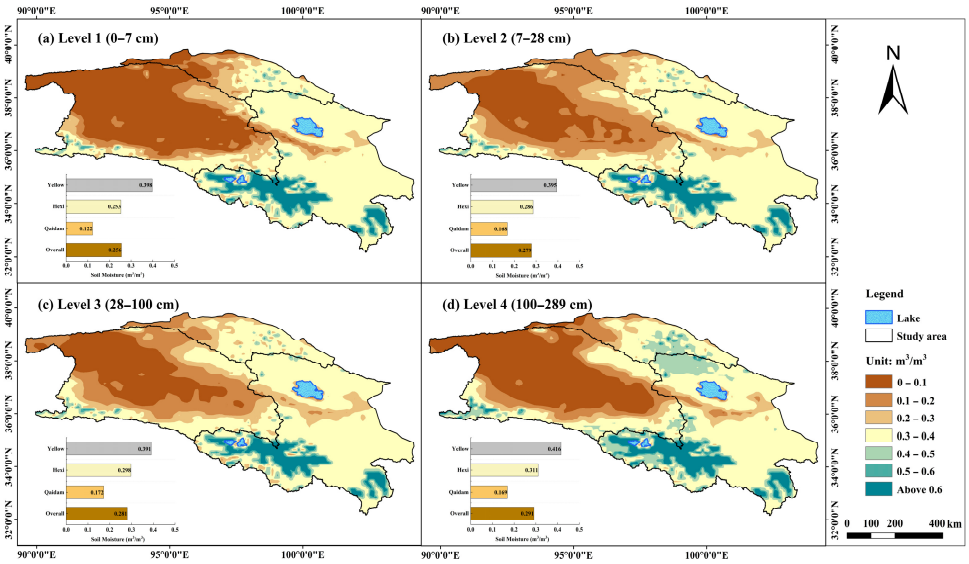

Figure 3. Spatial pattern of multi-year average moisture values across soil layers.

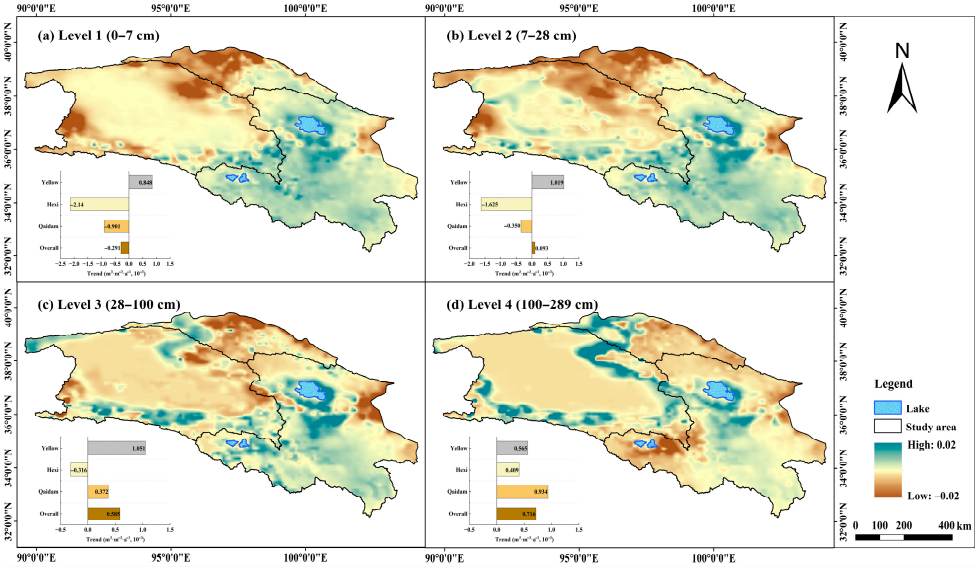

Figure 4. Variation trend in moisture values across soil layers.

To facilitate a more comprehensive comparison of the dynamic changes in soil water and salt transport, the annual data have been standardized with the Z-score method, shown in Figure 5. Although the variation trend in salt elements is relatively chaotic, there is a common characteristic in soil moisture across layers such that the research period can be divided into two different sub-periods. From 2013 to 2019, soil moisture shows an increasing fluctuation, while it shows an opposite decreasing fluctuation from 2020 to 2023.

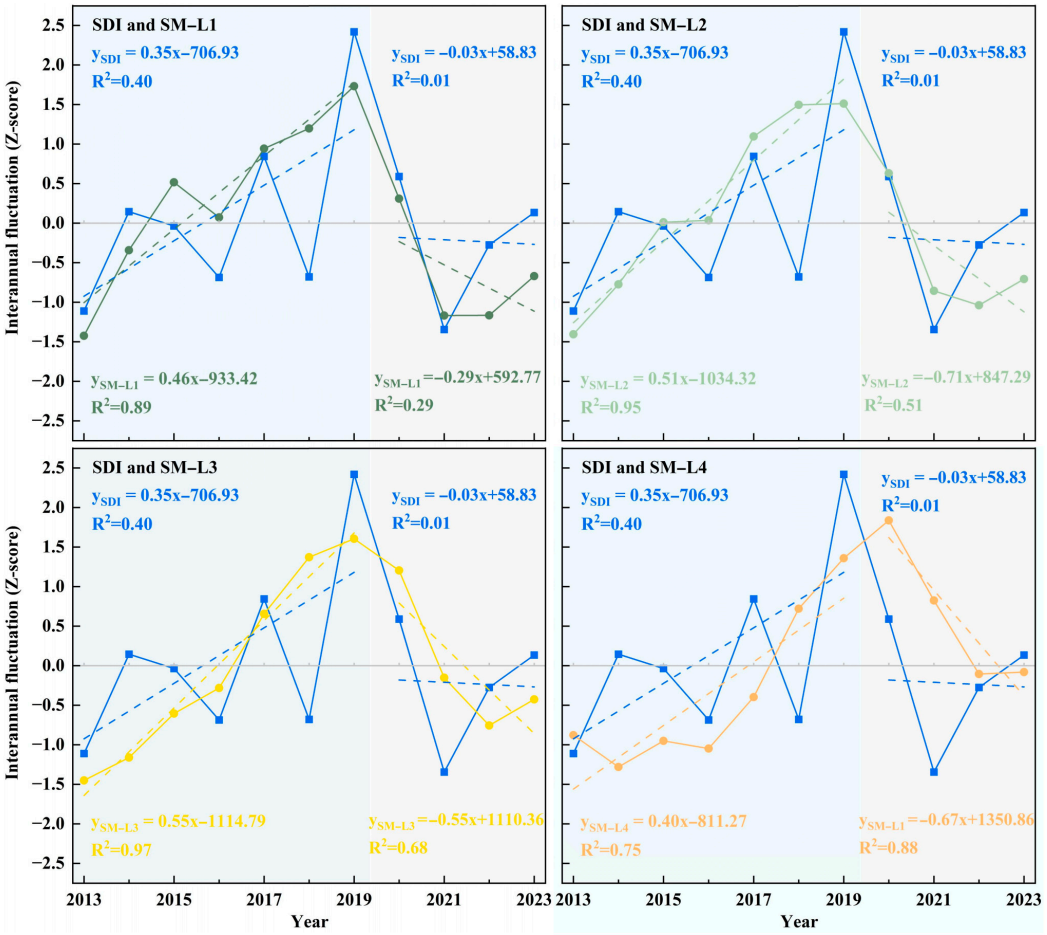

Figure 5. Interannual fluctuation of salinization detection index and soil moisture across layers. Solid lines represent interannual fluctuations, while the dashed lines represent the interannual trends fitted during two periods.

3.2. Time Lag Correlation

A pixel-by-pixel comparison has been conducted on the correlation between soil salinization and soil moisture across layers in the northeast Tibetan Plateau, and the results are shown in Figure 6. Overall, the main associated factor of soil salinization in this region is the Level 4 deep soil moisture, accounting for around 40% in all soil water and salt transport processes. The areas with soil moisture above the root zone (from Level 1 to Level 3) as the main parameter are mostly concentrated in the southeast and around Qinghai Lake. Similarly with Level 4 soil moisture as the dominant factor, Qaidam River Basin has the highest proportion, accounting for nearly half, followed by the Hexi River Basin (42%) and the Yellow River Basin (34%). Compared to other basins, the special habitat of the Qaidam River Basin leads to less disturbance from agricultural and pastoral activities, perhaps making soil water and salt transport in the region inclining towards natural evolution, causing Level 4 to become dominant in the transport process.

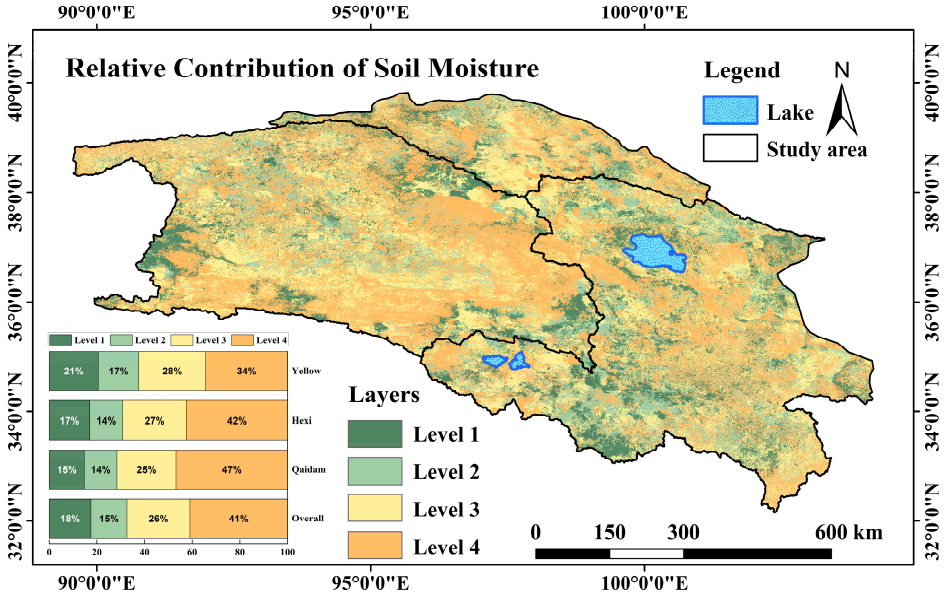

Figure 6. Relative contribution of soil moisture across layers for soil salinization.

Figure 7 shows the result of a sliding window experiment at a month scale within a complete hydrological year, and the time lag within one month to three months is considered as the cumulative effect on one seasonal period. Therefore, the whole sliding window period is divided into four seasonal duration periods. Different time lag results mean that soil water transport processes require a corresponding lasting time, only then leading to a feedback phenomenon of surface soil salinization. Compared with instant correlation, there is a time lag effect in the Level 1 layer; nevertheless, as the sliding window extends, the cumulative area proportion of the corresponding time lag effects in each seasonal period remains at around 20%. The time lag effect of the Level 2 layer and Level 3 layer has the highest proportion in the duration of the two seasonal periods (30.96% and 27.80%, respectively); it is speculated that the salinization phenomenon caused by soil water and salt transport affected by 7–100 cm soil moisture probably takes approximately six months. At the same time, the lag effect of the Level 4 layer has the highest proportion among the four seasonal periods (31.34%), suggesting that soil moisture below the crop root zone requires longer transport times to cause feedback on surface salinization.

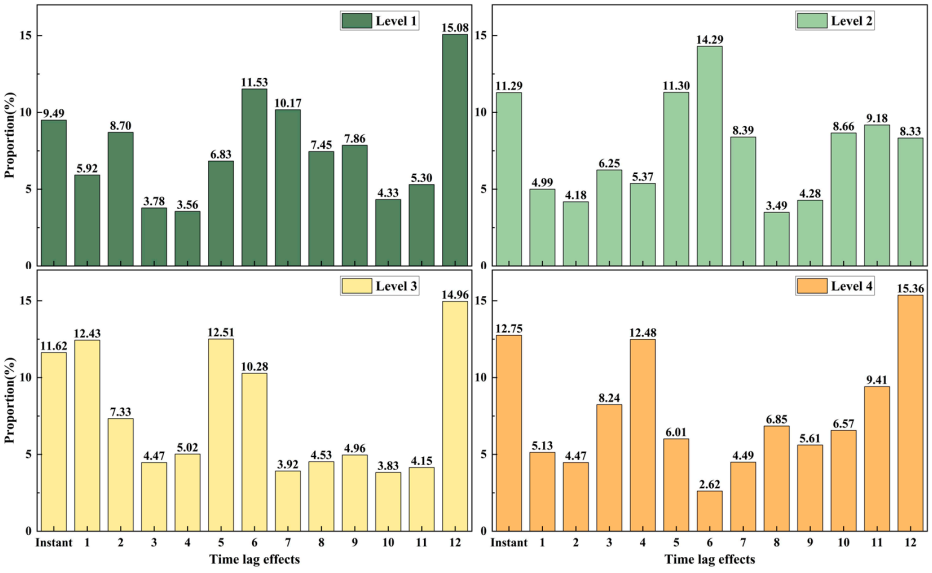

Figure 7. Windowed cross correlations between SDI and dominant soil moisture.

3.3. Potential Driving Factor Analysis

Several studies have demonstrated that climate factors including runoff [48] and surface solar radiation (SSR) [49], as well as soil texture including soil organic carbon (SOC) [50] and cation exchange capacity (CEC) [51], can both affect soil water and salt transport processes. Therefore, this study utilized the random forest algorithm and SHAP analysis to explore the regulation effects of four variables on the SDI and Level 4 layer deep soil moisture (DSM), which is the discovered critical element in the northeast Tibetan Plateau, including runoff, SSR, SOC, and CEC, as mentioned earlier.

Figure 8a,b shows the feature importance and the summary plot obtained from the experiment with the SDI as the explained variable, respectively. For the SDI, the feature importance from highest to lowest ranks as SOC > runoff > SSR > CEC. When SOC and runoff values increase, the negative regulation on the SDI becomes more pronounced, indicating that an increase in soil organic carbon and runoff is beneficial for alleviating soil salinization. When discussing DSM, runoff becomes the most critical variable with an explanatory power of over 80%, followed by SSR, while the two types of soil texture, SOC and CEC, have a non-significant influence, shown in Figure 8c. An increase in runoff will promote the humidification in deep soil, and the stable wetting phenomenon at lower surface solar radiation levels will be disrupted as radiation levels increase, inferred from Figure 8d.

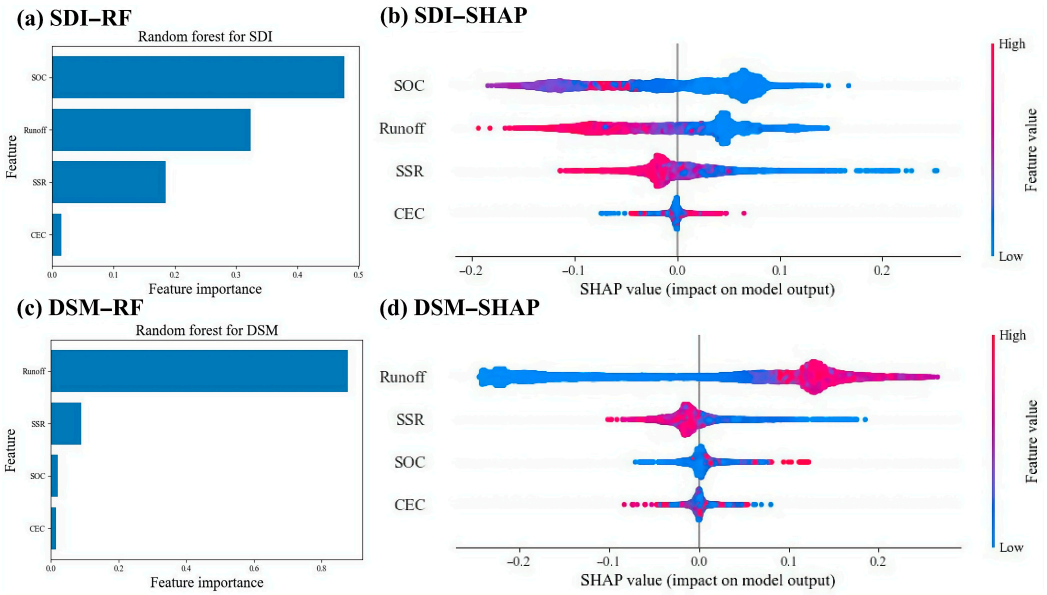

Figure 8. Driving factor identification combined machine learning for the salinization detection index (SDI) and deep soil moisture (DSM). Each row in the figure represents a feature, with the horizontal axis representing the SHAP value, and the features are sorted from high to low based on the absolute average SHAP value. The redder the color, the greater the numerical value of the feature itself, whereas a bluer color means the smaller the numerical value of the feature itself. Wide areas indicate a large concentration of samples.

When the soil organic carbon content is low, the soil structure becomes more compact, resulting in an uneven water infiltration. Soil salt accumulates on the surface as water evaporates, leading to an increase in surface soil salinity. In areas with relatively flat terrain or strong permeability, a large amount of infiltration is accompanied by runoff. Along with the infiltration into shallow soil, water can be more effectively transported to deep soil through the synergistic effect of gravity and capillary forces, promoting soil humidification. Therefore, using the dominant factors as environmental indicators can

scientifically understand its importance in maintaining regional soil water and salt balance, which has profound significance for ecological balance and sustainable development.

Furthermore, two climate factors have both spatial and temporal characteristics; similarly to soil water and salt elements, an in-depth exploration is conducted with the help of SHAP analysis, as shown in Figure 9. There is an evident negative relationship between runoff and the SDI, which means that the soil salinization extent gradually improves as runoff increases. After exceeding 4.08 m of equivalent, the increase in runoff at this time will lead to a significant decrease in the SDI. Simultaneously, the relationship between the SDI and SSR is mainly positive, indicating that high-intensity solar radiation can exacerbate soil salinization, while this intensification phenomenon will weaken after 150.15 $W \cdot m^{-2}$. Additionally, when runoff exceeds 3.91 m of equivalent, the deep soil humidification effect caused by increased runoff will become more pronounced. Similarly to it, the increase in surface solar radiation induces deep soil drying, and the threshold point for intensification appears at 141.62 $W \cdot m^{-2}$.

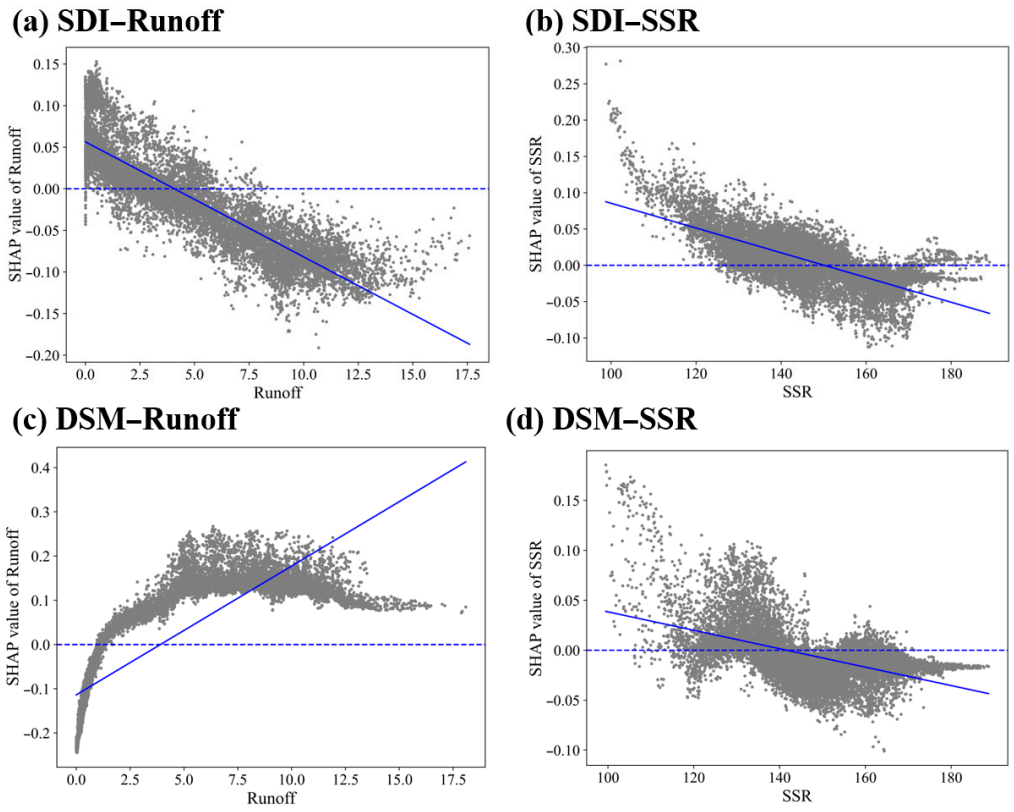

Figure 9. Turning point analysis of climatic element for SDI and DSM. Solid lines represent the linear fitting of the sample point distribution, while the dashed lines rep-resent the boundary line between the positive effect and negative effect of SHAP values.

4. Discussion

4.1. Result Robustness

As a satellite image covering the globe, the Landsat series has been proven to be a reliable basis for soil salinization mapping [52] and has empirical cases in specific areas [53]. Considering that there are no publicly available measured data on soil salinization in the Tibetan Plateau from 2013 to 2023, we have obtained the soil salinization observation data in the Syr Darya River Basin on May 2017 from the National Tibetan Plateau/Third Pole Environment Data Center (https://doi.org/10.11888/Soil.tpdc.270458, accessed on 21 November 2024). The observed values of soil salinization are processed, analyzed, and organized in accordance with the provisions of the agricultural industry standards

of the People's Republic of China (NY/T 1121.16-2006, Soil Testing Part 16: Method for determination of total water-soluble salt). Meanwhile, the salinization detection index has been calculated by the spectral data of the Landsat 8 OLI images within the region and has been compared with observation data at the same latitude and longitude position. The coefficient of determination (R^2) between the model results and the observed values achieves 0.7334 at a 95% confidence interval, as seen in the Supplementary Information, which indicates the goodness and accuracy of the salinization prediction. Similarly, utilizing the ERA5-Land reanalysis dataset to evaluate multiple profiles of soil moisture in the Tibetan Plateau has been strongly proven in several studies [54–56]. In comparison with other meteorological datasets, ERA5-Land also exhibits high accuracy, which achieves a correlation coefficient of above 0.7 with measured soil moisture data in general [57].

Although the acquisition and processing of remote sensing spectral data and meteorological reanalysis datasets are proposed to deviate from actual values (inevitable overestimation or occasional missing data), it remains a powerful explanatory tool. On the whole, the coupling of Landsat 8 OLI images and ERA5-Land data can reveal the spatiotemporal features of soil water and salt transport in the northeast Tibetan Plateau.

4.2. Fluctuation Similarity

The increase in soil moisture observed in the previous stage has also been validated in other studies [58,59], and the response of potential water sources and evapotranspiration conditions to climate change may be one of the reasons [60]. The increase in soil moisture could indicate that the synergy between atmospheric circulation and monsoon movement leads to the warming and humidification of Tibetan Plateau [61]. However, under the influence of global warming, changes in atmospheric circulation patterns have led to precipitation shortages and soil drought in the Tibetan Plateau [62]. This, together with unreasonable agricultural and pastoral activities, lead to a decrease in soil moisture in the second stage [63]. In addition, compared to the first three soil layers, the peak value of the Level 4 soil layer moisture lags slightly behind. The presence of plateau soil organic matter can alter soil properties and land atmosphere feedback, leading to the drying of near surface soil but cooling of deep soil [64], ultimately resulting in a delayed drying response of deep soil.

4.3. Dominant Factor Comparison

In previous studies, the dominant soil moisture which is most closely related to soil salinization may vary depending on study sites and evaluation periods. A study conducted in the Jiefangzha irrigation district of Inner Mongolia has demonstrated that the shallow soil moisture significantly affects the groundwater reflux process, leading to differential surface soil salinization [65]. However, in the Songnen Plain of Northeast China, which is covered with permafrost, the response relationship between soil water and soil salt is most significant at the critical soil freezing depth [66]. A field survey conducted in the Ebinur Lake Wetland National Nature Reserve has shown that soil salinization is regulated by deep soil moisture during the wet season and changes to shallow soil moisture during the dry season [67]. In our study, deep soil moisture plays a significant dominant role in regulating soil salinization in the northeast Tibetan Plateau. This may be related to the active evapotranspiration phenomenon in the region, where deep soil moisture transport is intensified to supply surface soil water and bring more soil salt to the surface.

4.4. Associated Ecological Threat

The transport of soil water and soil salt is crucial in plateau agroecosystems and is extremely sensitive to rapidly developing global climate change [68]. High concentrations of salt inhibit plant growth, leading to a decrease in vegetation coverage and species,

often threatening the stability and biodiversity of plateau agroecosystems and inducing more fragile habitats in the Tibetan Plateau [69]. With the continuous increase in salt lake quantity on the Tibetan Plateau [70], a large amount of saline water in the lake has overflowed [71], causing severe soil salinization and making it difficult for vegetation to grow [72]. Desertification and soil erosion occur consequently [73], causing the loss of mature substrate and declining fertility on the surface soil [74], further reducing the area of arable land and hindering the sustainable development of agroecosystems [75]. These together constitute the ecological threat of soil salinization for plateau agroecosystems; therefore, clarifying the basic process of water and salt transport is of great significance.

5. Conclusions

As an important component of agroecosystems, the process of soil water and salt transport determine soil endowment, and the associated soil salinization problem often affects sustainable agriculture development at the regional scale. This study couples multi-source remote sensing images to elucidate the regulation mechanism of soil salinization among typical basins in the northeast Tibetan Plateau. Several analytical methods are employed to comprehensively evaluate this complex process, such as spectral synthesis, a trend test, attribution assessment, time lag analysis, and dominant factor identification. The findings yield several key conclusions as follows:

(1) The soil salinization in the northeast Tibetan Plateau shows a space pattern increasing from southeast to northwest, with differentiation among river basins. Different profile data indicate that deep soil is more humid than shallow soil, and the variation trend is mostly manifested as drying in the shallow layer and wetting in the deep layer gradually.

(2) The main associated element of soil salinization in this region is Level 4 soil moisture, there is a time lag effect of soil moisture across layers on the regulation of soil salinization, and the window period of time lag effect for deep soil moisture is longer correspondingly.

(3) The influence of various driving factors on soil salinization and deep soil moisture are different. An increase in soil organic carbon and runoff helps alleviate salinization, while habitat conditions with abundant runoff and low-level surface solar radiation are more conducive to deep soil humidification.

Supplementary Materials: The relevant statements about the ground truthing of salinization detection index are shown in the supplementary information. The following supporting information can be downloaded at: https://www.mdpi.com/article/10.3390/agriculture15010106/s1, Figure S1: Fitting curve of measured soil salt content and calculated SDI; Table S1: Comparison between measured soil salt content and calculated SDI.

Author Contributions: D.W., conceptualization, investigation, writing—original draft; Z.Z., data curation, investigation, writing—original draft; L.Y., validation; J.Y., investigation, validation; Y.Z., writing—reviewing and editing; B.W., supervision. All authors have read and agreed to the published version of the manuscript.

Funding: This research was funded by the Gansu Province Ecological Civilization Construction Key R&D Projects (no. 24YFFA004), Gansu Province Young Talent Team Project, Department of Education of Gansu Province: Major cultivation project of scientific research innovation platform in university (2024CXPT-14).

Institutional Review Board Statement: Not applicable.

Data Availability Statement: Publicly available datasets were analyzed in this study. The data for analysis within this article (satellite images, soil moisture across layers, driving factors) were downloaded and processed using Google Earth Engine (https://earthengine.google.org, accessed on 30 May 2024).

Conflicts of Interest: The authors declare no conflicts of interest.

References

1. Jiang, D.; Ao, C.; Bailey, R.T.; Zeng, W.; Huang, J. Simulation of water and salt transport in the Kaidu River Irrigation District using the modified SWAT-Salt. *Agric. Water Manag.* **2022**, *272*, 107845. [CrossRef]
2. Zhang, X.; Shu, C.; Fujii, M.; Wu, Y.; Ye, P.; Bao, Y. Numerical and experimental study on water-heat-salt transport patterns in shallow bare soil with varying salt contents under evaporative conditions: A comparative investigation. *J. Hydrol.* **2023**, *621*, 129564. [CrossRef]
3. Lee, X.; Yang, F.; Xing, Y.; Huang, Y.; Xu, L.; Liu, Z.; Holtzman, R.; Kan, I.; Li, Y.; Zhang, L. Use of biochar to manage soil salts and water: Effects and mechanisms. *Catena* **2022**, *211*, 106018. [CrossRef]
4. Daba, A.W.; Qureshi, A.S. Review of soil salinity and sodicity challenges to crop production in the lowland irrigated areas of Ethiopia and its management strategies. *Land* **2021**, *10*, 1377. [CrossRef]
5. Dong, X.; Ding, J.; Ge, X. Future changes in soil salinization across Central Asia under CMIP6 forcing scenarios. *Land Degrad. Dev.* **2024**, *35*, 3981–3998. [CrossRef]
6. Fan, G.; Zhang, D.; Zhang, J.; Li, Z.; Sang, W.; Zhao, L.; Xu, M. Ecological environmental effects of Yellow River irrigation revealed by isotope and ion hydrochemistry in the Yinchuan Plain, Northwest China. *Ecol. Indic.* **2022**, *135*, 108574. [CrossRef]
7. Liu, Y.; Han, X.; Zhu, Y.; Li, H.; Qian, Y.; Wang, K.; Ye, M. Spatial mapping and driving factor Identification for salt-affected soils at continental scale using Machine learning methods. *J. Hydrol.* **2024**, *639*, 131589. [CrossRef]
8. Jia, P.; Zhang, J.; Liang, Y.; Zhang, S.; Jia, K.; Zhao, X. The inversion of arid-coastal cultivated soil salinity using explainable machine learning and Sentinel-2. *Ecol. Indic.* **2024**, *166*, 112364. [CrossRef]
9. Santi, E.; Comite, D.; Dente, L.; Guerriero, L.; Pierdicca, N.; Clarizia, M.P.; Floury, N. Global soil moisture mapping at 5 km by combining GNSS reflectometry and machine learning in view of HydroGNSS. *Sci. Remote Sens.* **2024**, *10*, 100177. [CrossRef]
10. Singh, A.; Gaurav, K. PIML-SM: Physics-informed machine learning to estimate surface soil moisture from multi-sensor satellite images by leveraging swarm intelligence. *IEEE Trans. Geosci. Remote Sens.* **2024**, *62*, 4416913. [CrossRef]
11. Zhang, J.; Cai, J.; Xu, D.; Wu, B.; Chang, H.; Zhang, B.; Wei, Z. Soil salinization poses greater effects than soil moisture on field crop growth and yield in arid farming areas with intense irrigation. *J. Clean. Prod.* **2024**, *451*, 142007. [CrossRef]
12. Xiao, J.; Chevallier, F.; Gomez, C.; Guanter, L.; Hicke, J.A.; Huete, A.R.; Ichii, K.; Ni, W.; Pang, Y.; Rahman, A.F. Remote sensing of the terrestrial carbon cycle: A review of advances over 50 years. *Remote Sens. Environ.* **2019**, *233*, 111383. [CrossRef]
13. Mello, D.C.; Ferreira, T.O.; Veloso, G.V.; de Lana, M.G.; de Oliveira Mello, F.A.; Di Raimo, L.A.D.L.; Schaefer, C.E.G.R.; Francelino, M.R.; Fernandes-Filho, E.I.; Demattê, J.A. Pedogenetic processes operating at different intensities inferred by geophysical sensors and machine learning algorithms. *Catena* **2022**, *216*, 106370. [CrossRef]
14. Hassani, A.; Azapagic, A.; Shokri, N. Global predictions of primary soil salinization under changing climate in the 21st century. *Nat. Commun.* **2021**, *12*, 6663. [CrossRef] [PubMed]
15. Metternicht, G.I.; Zinck, J. Remote sensing of soil salinity: Potentials and constraints. *Remote Sens. Environ.* **2003**, *85*, 1–20. [CrossRef]
16. Singh, A. Soil salinity: A global threat to sustainable development. *Soil Use Manag.* **2022**, *38*, 39–67. [CrossRef]
17. Smanov, Z.M.; Laiskhanov, S.U.; Poshanov, M.N.; Abikbayev, Y.R.; Duisekov, S.N.; Tulegenov, Y.A. Mapping of cornfield soil salinity in arid and semi-arid regions. *J. Ecol. Eng.* **2023**, *24*, 146–158. [CrossRef]
18. Avdan, U.; Kaplan, G.; Matcı, D.K.; Avdan, Z.Y.; Erdem, F.; Mızık, E.T.; Demirtaş, İ. Soil salinity prediction models constructed by different remote sensors. *Phys. Chem. Earth Parts A/B/C* **2022**, *128*, 103230. [CrossRef]
19. Sahbeni, G.; Ngabire, M.; Musyimi, P.K.; Székely, B. Challenges and opportunities in remote sensing for soil salinization mapping and monitoring: A review. *Remote Sens.* **2023**, *15*, 2540. [CrossRef]
20. Pfitzner, K.S.; Harford, A.J.; Whiteside, T.G.; Bartolo, R.E. Mapping magnesium sulfate salts from saline mine discharge with airborne hyperspectral data. *Science of The Total Environment* **2018**, *640*, 1259–1271. [CrossRef]
21. Liu, Y.; Qian, J.; Yue, H. Comparison and evaluation of different dryness indices based on vegetation indices-land surface temperature/albedo feature space. *Adv. Space Res.* **2021**, *68*, 2791–2803. [CrossRef]
22. Ding, J.; Qu, J.; Sun, Y.; Zhang, Y. The retrieval model of soil salinization information in arid region based on MSAVI-WI feature space: A case study of the delta oasis in Weigan-Kuqa watershed. *Geogr. Res.* **2013**, *32*, 223–232.
23. Bian, L.; Wang, J.; Guo, B.; Cheng, K.; Wei, H. Remote sensing extraction of soil salinity in Yellow River Delta Kenli County based on feature space. *Remote Sens. Technol. Appl.* **2020**, *35*, 211–218.
24. Jiang, Z.; Hao, Z.; Ding, J.; Miao, Z.; Zhang, Y.; Alimu, A.; Jin, X.; Cheng, H.; Ma, W. Weighted Variable Optimization-Based Method for Estimating Soil Salinity Using Multi-Source Remote Sensing Data: A Case Study in the Weiku Oasis, Xinjiang, China. *Remote Sens.* **2024**, *16*, 3145. [CrossRef]
25. Merembayev, T.; Amirgaliyev, Y.; Saurov, S.; Wójcik, W. Soil salinity classification using machine learning algorithms and radar data in the case from the South of Kazakhstan. *J. Ecol. Eng.* **2022**, *23*, 61–67. [CrossRef]

26. Yan, Y.; Guan, Q.; Shao, W.; Wang, Q.; Yang, X.; Luo, H. Spatiotemporal dynamics and driving mechanism of arable ecosystem stability in arid and semi-arid areas based on Pressure-Buffer-Response process. *J. Clean. Prod.* **2023**, *421*, 138553. [CrossRef]
27. Habibi, V.; Ahmadi, H.; Jafari, M.; Moeini, A. Mapping soil salinity using a combined spectral and topographical indices with artificial neural network. *PLoS ONE* **2021**, *16*, e0228494. [CrossRef] [PubMed]
28. Lin, Q.; Xu, L.; Hou, J.; Liu, Z.; Jeppesen, E.; Han, B.-P. Responses of trophic structure and zooplankton community to salinity and temperature in Tibetan lakes: Implication for the effect of climate warming. *Water Res.* **2017**, *124*, 618–629. [CrossRef] [PubMed]
29. Zhaofeng, W.; Hartemink, A.E.; Zhang, Y.; Zhang, H.; Mingjun, D. Major elements in soils along a 2.8–km altitudinal gradient on the Tibetan Plateau, China. *Pedosphere* **2016**, *26*, 895–903.
30. Yao, G.; Li, L.; Cai, M.; Liu, Y. Mechanisms of salinization in a middle Eocene lake in the Tanggu area of the Huanghua Depression. *Mar. Pet. Geol.* **2017**, *86*, 155–167. [CrossRef]
31. Okin, G.S.; D'Odorico, P.; Liu, J. A Mechanism of Land Degradation in Turf-Mantled Slopes of the Tibetan Plateau. *Geophys. Res. Lett.* **2018**, *45*, 4041–4048. [CrossRef]
32. Zhang, G.; Yao, T.; Xie, H.; Yang, K.; Zhu, L.; Shum, C.; Bolch, T.; Yi, S.; Allen, S.; Jiang, L. Response of Tibetan Plateau lakes to climate change: Trends, patterns, and mechanisms. *Earth-Sci. Rev.* **2020**, *208*, 103269. [CrossRef]
33. Li, M.; Liu, S.; Sun, Y.; Liu, Y. Agriculture and animal husbandry increased carbon footprint on the Qinghai-Tibet Plateau during past three decades. *J. Clean. Prod.* **2021**, *278*, 123963. [CrossRef]
34. Barreto, A.C.; Neto, M.F.; de Oliveira, R.P.; Moreira, L.C.J.; de Medeiros, J.F.; da Silva Sá, F.V. Comparative analysis of spectral indexes for soil salinity mapping in irrigated areas in a semi-arid region, Brazil. *J. Arid. Environ.* **2023**, *209*, 104888. [CrossRef]
35. Wei, D.; Zhang, Y.; Li, Y.; Zhang, Y.; Wang, B. Hydrothermal Conditions in Deep Soil Layer Regulate the Interannual Change in Gross Primary Productivity in the Qilian Mountains Area, China. *Forests* **2023**, *14*, 2422. [CrossRef]
36. Muñoz-Sabater, J.; Dutra, E.; Agustí-Panareda, A.; Albergel, C.; Arduini, G.; Balsamo, G.; Boussetta, S.; Choulga, M.; Harrigan, S.; Hersbach, H. ERA5-Land: A state-of-the-art global reanalysis dataset for land applications. *Earth Syst. Sci. Data* **2021**, *13*, 4349–4383. [CrossRef]
37. Guo, B.; Yang, F.; Han, B.; Fan, Y.; Chen, S.; Yang, W.; Jiang, L. A model for the rapid monitoring of soil salinization in the Yellow River Delta using Landsat 8 OLI imagery based on VI-SI feature space. *Remote Sens. Lett.* **2019**, *10*, 796–805. [CrossRef]
38. Sen, P.K. Estimates of the regression coefficient based on Kendall's tau. *J. Am. Stat. Assoc.* **1968**, *63*, 1379–1389. [CrossRef]
39. Zhang, S.; Liu, S.; Mo, X.; Shu, C.; Sun, Y.; Zhang, C. Assessing the impact of climate change on potential evapotranspiration in Aksu River Basin. *J. Geogr. Sci.* **2011**, *21*, 609–620. [CrossRef]
40. Walker, E.; Birch, J.B. Influence measures in ridge regression. *Technometrics* **1988**, *30*, 221–227. [CrossRef]
41. Zhao, Y.; Chen, Y.; Wu, C.; Li, G.; Ma, M.; Fan, L.; Zheng, H.; Song, L.; Tang, X. Exploring the contribution of environmental factors to evapotranspiration dynamics in the Three-River-Source region, China. *J. Hydrol.* **2023**, *626*, 130222. [CrossRef]
42. Boker, S.M.; Rotondo, J.L.; Xu, M.; King, K. Windowed cross-correlation and peak picking for the analysis of variability in the association between behavioral time series. *Psychol. Methods* **2002**, *7*, 338. [CrossRef] [PubMed]
43. Yang, X.; Zhang, Z.; Guan, Q.; Zhang, E.; Sun, Y.; Yan, Y.; Du, Q. Coupling mechanism between vegetation and multi-depth soil moisture in arid–semiarid area: Shift of dominant role from vegetation to soil moisture. *For. Ecol. Manag.* **2023**, *546*, 121323. [CrossRef]
44. Georganos, S.; Grippa, T.; Vanhuysse, S.; Lennert, M.; Shimoni, M.; Kalogirou, S.; Wolff, E. Less is more: Optimizing classification performance through feature selection in a very-high-resolution remote sensing object-based urban application. *GISci. Remote Sens.* **2018**, *55*, 221–242. [CrossRef]
45. Scornet, E.; Biau, G.; Vert, J.P. Consistency of random forests. *Ann. Stat.* **2015**, *43*, 1716–1741. [CrossRef]
46. Lundberg, S.M.; Erion, G.; Chen, H.; DeGrave, A.; Prutkin, J.M.; Nair, B.; Katz, R.; Himmelfarb, J.; Bansal, N.; Lee, S.-I. From local explanations to global understanding with explainable AI for trees. *Nat. Mach. Intell.* **2020**, *2*, 56–67. [CrossRef] [PubMed]
47. Chang, I.; Park, H.; Hong, E.; Lee, J.; Kwon, N. Predicting effects of built environment on fatal pedestrian accidents at location-specific level: Application of XGBoost and SHAP. *Accid. Anal. Prev.* **2022**, *166*, 106545. [CrossRef] [PubMed]
48. Zhang, Y.; Hou, K.; Qian, H.; Gao, Y.; Fang, Y.; Tang, S.; Xiao, S.; Ren, W.; Qu, W.; Zhang, Q. Natural-human driving factors of groundwater salinization in a long-term irrigation area. *Environ. Res.* **2023**, *220*, 115178. [CrossRef] [PubMed]
49. Khamidov, M.; Ishchanov, J.; Hamidov, A.; Shermatov, E.; Gafurov, Z. Impact of soil surface temperature on changes in the groundwater level. *Water* **2023**, *15*, 3865. [CrossRef]
50. Zhou, T.; Wang, Z.; Lv, Q.; Zhang, Y.; Tao, S.; Ren, X.; Gao, H.; Gao, Z.; Hu, S. Sulfur dynamics in saline sodic soils: The role of paddy cultivation and organic amendments. *Ecol. Indic.* **2024**, *162*, 112014. [CrossRef]
51. Hou, R.; Qi, Z.; Li, T.; Fu, Q.; Meng, F.; Liu, D.; Li, Q.; Zhao, H.; Yu, P. Mechanism of snowmelt infiltration coupled with salt transport in soil amended with carbon-based materials in seasonally frozen areas. *Geoderma* **2022**, *420*, 115882. [CrossRef]
52. Guo, B.; Lu, M.; Fan, Y.; Wu, H.; Yang, Y.; Wang, C. A novel remote sensing monitoring index of salinization based on three-dimensional feature space model and its application in the Yellow River Delta of China. *Geomat. Nat. Hazards Risk* **2023**, *14*, 95–116. [CrossRef]

53. Li, L.; Ni, W.; Li, T.; Zhou, B.; Qu, Y.; Yuan, K. Influences of anthropogenic factors on lakes area in the Golmud Basin, China, from 1980 to 2015. *Environ. Earth Sci.* **2020**, *79*, 20. [CrossRef]
54. Liu, Y.; Yang, Y. Multi-depth evolution characteristics of soil moisture over the Tibetan Plateau in the past 70 years using reanalysis products. *Front. Environ. Sci.* **2022**, *10*, 979853. [CrossRef]
55. Sun, G.; Hu, Z.; Ma, Y.; Xie, Z.; Sun, F.; Wang, J.; Yang, S. Analysis of local land atmosphere coupling characteristics over Tibetan Plateau in the dry and rainy seasons using observational data and ERA5. *Sci. Total Environ.* **2021**, *774*, 145138. [CrossRef]
56. Yang, S.; Li, R.; Wu, T.; Hu, G.; Xiao, Y.; Du, Y.; Zhu, X.; Ni, J.; Ma, J.; Zhang, Y. Evaluation of reanalysis soil temperature and soil moisture products in permafrost regions on the Qinghai-Tibetan Plateau. *Geoderma* **2020**, *377*, 114583. [CrossRef]
57. Wang, H.; Zan, B.; Wei, J.; Song, Y.; Mao, Q. Spatiotemporal characteristics of soil Moisture and land–atmosphere coupling over the Tibetan Plateau derived from three gridded datasets. *Remote Sens.* **2022**, *14*, 5819. [CrossRef]
58. Ji, Y.; Li, Y.; Yao, N.; Biswas, A.; Zou, Y.; Meng, Q.; Liu, F. The lagged effect and impact of soil moisture drought on terrestrial ecosystem water use efficiency. *Ecol. Indic.* **2021**, *133*, 108349. [CrossRef]
59. Li, Z.; Li, X.; Yang, S. Plant drought adaptation strategies regulate alpine grassland water yield in the Qinghai Lake Basin, northeastern Qinghai-Tibet Plateau. *J. Hydrol. Reg. Stud.* **2023**, *48*, 101470. [CrossRef]
60. Lin, H.; Yu, Z.; Chen, X.; Gu, H.; Ju, Q.; Shen, T. Spatial-temporal dynamics of meteorological and soil moisture drought on the Tibetan Plateau: Trend, response, and propagation process. *J. Hydrol.* **2023**, *626*, 130211. [CrossRef]
61. Ullah, W.; Wang, G.; Lou, D.; Gao, Z.; Zhu, C.; Samuel Bhatti, A.; Tawia Hagan, D.F.; Li, S.; Jiang, T.; Su, B. The Empirical Influence of Tibetan Plateau Spring Soil Moisture on South Asian Monsoon Onset: A Linear Diagnostic Perspective. *J. Clim.* **2023**, *36*, 8723–8742. [CrossRef]
62. Gu, Z.; Gu, L.; Yin, J.; Fang, W.; Xiong, L.; Guo, J.; Zeng, Z.; Xia, J. Impact of atmospheric circulations on droughts and drought propagation over China. *Sci. China Earth Sci.* **2024**, *67*, 2633–2648. [CrossRef]
63. Tian, Y.; Jiang, G.; Zhou, D.; Li, G. Heterogeneity and regional differences in ecosystem services responses driven by the "Three Modernizations". *Land Degrad. Dev.* **2021**, *32*, 3743–3761. [CrossRef]
64. Sun, J.; Yang, K.; Lu, H.; Zhou, X.; Li, X.; Chen, Y.; Guo, W.; Wright, J.S. Land–atmosphere feedbacks weaken the cooling effect of soil organic matter property toward deep soil on the eastern Tibetan Plateau. *J. Hydrometeorol.* **2023**, *24*, 105–117. [CrossRef]
65. Liu, Z.; Chen, H.; Huo, Z.; Wang, F.; Shock, C.C. Analysis of the contribution of groundwater to evapotranspiration in an arid irrigation district with shallow water table. *Agric. Water Manag.* **2016**, *171*, 131–141. [CrossRef]
66. Hou, R.; Li, T.-x.; Fu, Q.; Liu, D.; Li, M.; Zhou, Z.-q.; Yan, J.-w.; Zhang, S. Research on the distribution of soil water, heat, salt and their response mechanisms under freezing conditions. *Soil Tillage Res.* **2020**, *196*, 104486. [CrossRef]
67. Wang, Z.; Zhang, F.; Zhang, X.; Chan, N.W.; Kung, H.-t.; Zhou, X.; Wang, Y. Quantitative evaluation of spatial and temporal variation of soil salinization risk using GIS-based geostatistical method. *Remote Sens.* **2020**, *12*, 2405. [CrossRef]
68. Chen, Z.; Yu, D.; Cao, G.; Chen, K.; Fu, J.; Ma, Y.; Wang, X. Characteristics of Soil Temperature, Humidity, and Salinity on Bird Island within Qinghai Lake Basin, China. *Sustainability* **2022**, *14*, 9449. [CrossRef]
69. Chen, X.; Diao, H.; Wang, S.; Li, H.; Wang, Z.; Shen, Y.; Degen, A.A.; Dong, K.; Wang, C. Plant community mediated methane uptake in response to increasing nitrogen addition level in a saline-alkaline grassland by rhizospheric effects. *Geoderma* **2023**, *429*, 116235. [CrossRef]
70. Sun, Y.; Li, Y.; Li, L.; He, H. Preservation of cyanobacterial UVR-shielding pigment scytonemin in carbonate ooids formed in Pleistocene salt lakes in the Qaidam Basin, Tibetan Plateau. *Geophys. Res. Lett.* **2019**, *46*, 10375–10383. [CrossRef]
71. Fang, J.; Li, G.; Rubinato, M.; Ma, G.; Zhou, J.; Jia, G.; Yu, X.; Wang, H. Analysis of long-term water level variations in Qinghai Lake in China. *Water* **2019**, *11*, 2136. [CrossRef]
72. Ma, M.; Zhou, X.; Ma, Z.; Du, G. Composition of the soil seed bank and vegetation changes after wetland drying and soil salinization on the Tibetan Plateau. *Ecol. Eng.* **2012**, *44*, 18–24. [CrossRef]
73. Zhang, N.N.; Sun, G.; Zhong, B.; Wang, E.T.; Zhao, C.Z.; Wang, Y.J.; Cheng, W.; Wu, N. Impacts of wise grazing on physicochemical and biological features of soil in a sandy grassland on the Tibetan Plateau. *Land Degrad. Dev.* **2019**, *30*, 719–729. [CrossRef]
74. Cui, J.; Li, Y.; Adamowski, J.F.; Cao, J.; Biswas, A.; Wang, J.; Zhang, X. Response of leaf, litter, and root ecological stoichiometries to grazing exclosure duration on the Qinghai-Tibetan Plateau. *Soil Tillage Res.* **2024**, *241*, 106123. [CrossRef]
75. Yang, M.; Dong, S.; Dong, Q.; Xu, Y.; Zhi, Y.; Liu, W.; Zhao, X. Trade-offs in ecological, productivity and livelihood dimensions inform sustainable grassland management: Case study from the Qinghai-Tibetan Plateau. *Agric. Ecosyst. Environ.* **2021**, *313*, 107377. [CrossRef]